Tropical-extratropical linkages drove western United States lake expansions during Heinrich stadials

David McGee[1,*], Eduardo Moreno-Chamarro[1,2], John Marshall[1], Eric Galbraith[3,4]

[1]Department of Earth, Atmospheric and Planetary Sciences, Massachusetts Institute of Technology, Cambridge, MA 02139

[2]Barcelona Supercomputing Center (BSC), 08034 Barcelona, Spain

[3]Institut de Ciència i Tecnologia Ambientals (ICTA) and Department of Mathematics, Universitat Autonoma de Barcelona, 08193 Barcelona, Spain

[4]ICREA, Pg. Lluís Companys 23, 08010 Barcelona, Spain

[*]Corresponding author: davidmcg@mit.edu

Lake and cave records point to substantial increases in winter precipitation in the southwestern U.S. and Great Basin during millennial-scale periods of Northern Hemisphere cooling known as Heinrich stadials. The most recent highstands of most Great Basin paleolakes occurred during Heinrich Stadial 1, 18-14.7 kyr ago. Studies have variously associated these precipitation increases with southward shifts of the mid-latitude jet over the North Pacific, intensification of the jet, deepening of the Aleutian Low, and increases in summer monsoon precipitation and have disagreed as to the drivers of these atmospheric circulation changes. Drawing on the dynamics of modern interannual variability and a set of climate model simulations of North Atlantic cooling, we show that maximum winter precipitation anomalies are related to an intensified and slightly southward-shifted jet and a deepened and southeastward shifted Aleutian Low. The combination of jet and Aleutian Low changes increases atmospheric river-like transport of subtropical moisture into the western U.S., consistent with the spatial and temporal patterns we identify in lake level records. We further argue that the jet and Aleutian Low changes are directly related to the magnitude by which the Intertropical Convergence Zone (ITCZ) shifts south in the central Pacific, consistent with the understanding that a southward-shifted ITCZ and intensified local Hadley circulation increase angular momentum transports into the jet and drive wave responses that deepen and shift low pressures in the North Pacific. This mechanism directly ties changes in western U.S. water balance during Heinrich stadials to southward shifts of the Pacific ITCZ, expanding our understanding of the global atmospheric changes accompanying Heinrich stadials and highlighting the importance of accurate representations of

low-latitude teleconnections in model-based projections of future regional precipitation.

The winter precipitation-dominated portion of the southwestern U.S. extending from California through the Great Basin is a water-stressed region in which ongoing climate change is robustly projected to produce drier conditions in the annual mean in coming decades. Substantial uncertainties remain, however, in the magnitude and spatial extent of this drying due to uncertainty in the circulation responses to future climate change[1,2]. For over a century, ancient shoreline deposits in hydrologically closed basins within the U.S. Great Basin, spanning southern California through northern Utah, have been understood to indicate that the region experienced much wetter conditions in the past[3,4]. Water budget analyses have identified that these lake highstands require substantially increased precipitation (factor of ~2 relative to present) in addition to reduced evaporation[5–7]. These dramatic past changes in precipitation provide an important opportunity to identify the atmosphere's response to past climate changes, to test whether climate models produce realistic changes in precipitation when run with paleoclimate boundary conditions[8], and to better understand the dynamical mechanisms involved in present and future precipitation changes in the region.

Because of the approximate correspondence of lake highstands with the end of the last glacial period, early work to understand precipitation maxima in the southwestern U.S. focused on the impact of North American ice sheets on the jet stream[9,10]. Climate model simulations have consistently shown a southward deflection of a portion of the North Pacific jet stream by ice sheet topography, supporting a role for large ice sheets in driving increased winter precipitation in the Great Basin[10,11]. Improved chronologies for both ice extent and lake highstands over the last three decades, however, have demonstrated that the wettest conditions in the Great Basin did not occur during the time of maximum ice extent (the Last Glacial Maximum, or LGM, ~19-26 ka). Instead, most lakes reached their maximum extents during Heinrich Stadial 1 (HS1; ~18-14.7 ka)[12–14], a period of intense cooling of the North Atlantic and a southward shift of the Intertropical Convergence Zone (ITCZ)[15–17]. As reviewed below, recent evidence indicates that other Heinrich stadials were also marked by increased precipitation in the Great Basin, suggesting a consistent pattern.

Previous studies have suggested a range of changes in regional atmospheric circulation that could have increased precipitation in the southwestern U.S. during Heinrich stadials, including a southward shift of the jet[18], deepening of the Aleutian Low[19], increases in jet intensity[20,21], and increased summer precipitation[22]. Together, these results paint a confusing picture, with each study pointing to different aspects of the North Pacific atmospheric circulation. Moreover, these studies disagree as to whether the circulation changes leading to increased precipitation were driven by high-latitude cooling[18], changes in the Pacific ITCZ and Hadley circulation[21], or teleconnections to tropical Atlantic convection[23]. Here we draw on paleoclimate data, dynamics observed in modern interannual variability, and climate model simulations of North Atlantic cooling to provide a physical mechanism that integrates these previous results and substantially clarifies the drivers and patterns of precipitation and atmospheric circulation changes in the North Pacific and southwestern U.S. during Heinrich stadials.

Evidence for precipitation changes in the Great Basin during Heinrich stadials

We compiled Great Basin lake highstand ages to provide constraints on mechanisms of precipitation increases during Heinrich stadials. Though the most recent highstands occurred predominantly during HS1[13], these highstands were not synchronous (Figure 1). Highstands occurred along southwest-northeast trends and progressed through time from southeast to northwest. Basins in the southwest, center and northeast of the Great Basin attained their highstands between 16.0-17.5 ka, with many clustering around 16.5-17 ka. To the north and west of this southwest-northeast band, Lake Russell and Lake Lahontan reached their highstands slightly later, at 15.9-16.0 ka[13,24,25]. Moving farther to the northwest, the highstand at Lake Surprise (northeastern California) occurred at 15.2 ± 0.2 ka[6], and the highstand in the Chewaucan Basin (southeastern Oregon) in the far northwest of the Great Basin occurred after 14.6 ± 0.3 ka[26]. (For more detail on the highstand ages summarized in Figure 1, see the Supplementary Text.)

This pattern suggests that anomalous moisture supply was derived from the southwest and transported toward the northeast, consistent with a previous compilation of paleo-data spanning the deglaciation[22] while adding improved chronological control and newer records. The data are consistent with an amplification of southwesterly 'atmospheric river' moisture transport identified in LGM climate model simulations[27] but are oriented orthogonally to the northwest-southeast steering of LGM storms suggested by Oster et al.[28]. Northwestward progression of lake highstands during and immediately after HS1 could reflect the waning influence of ice sheet topography on the Pacific winter jet and Aleutian Low as the deglaciation progressed[20].

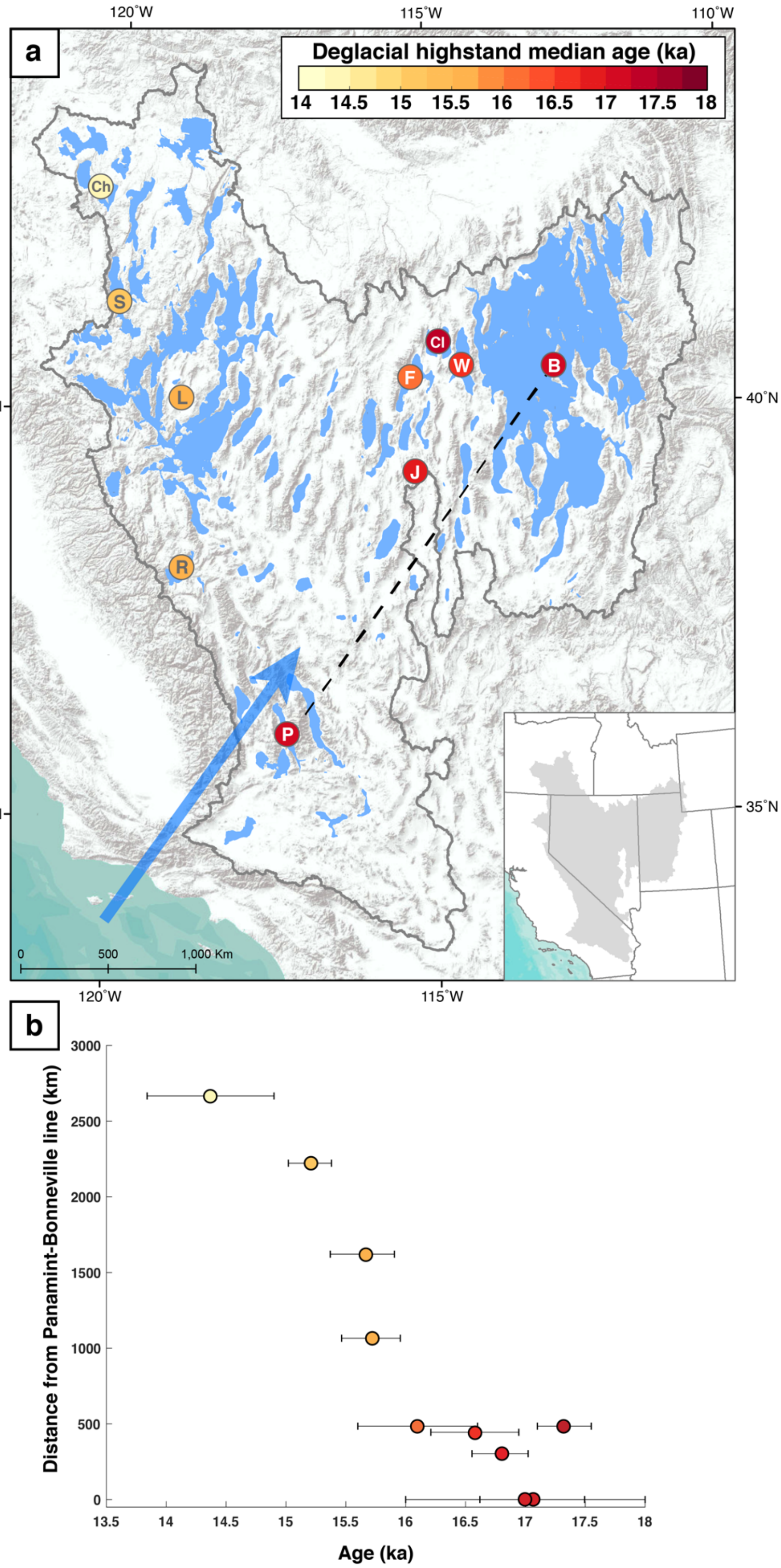
a
Deglacial highstand median age (ka)
14 14.5 15 15.5 16 16.5 17 17.5 18
120°W
115°W
110°W
40°N
35°N
Ch
S
L
R
P
Cl
W
F
B
J
0 500 1,000 Km
b
Distance from Panamint-Bonneville line (km)
Age (ka)
0 500 1000 1500 2000 2500 3000
13.5 14 14.5 15 15.5 16 16.5 17 17.5 18

Figure 1. Extents and ages of lake highstands in the U.S. Great Basin during the last deglaciation. a) Blue shading shows lakes at their greatest extents of the last glacial cycle. Colors denote timing of wettest conditions during the last deglaciation in each basin with sufficient dating confidence. Blue arrow shows direction of anomalous moisture transport during the first half of HS1 inferred from ages of lake highstands. Grey line is the outline of the Great Basin. Inset shows Great Basin outline with state boundaries. Paleolakes: B: Bonneville; Ch: Chewaucan; Cl: Clover; F: Franklin; J: Jakes; L: Lahontan; P: Panamint; R: Russell; S: Surprise; W: Waring. Lake highstand map adapted from [52]. **b)** Age estimates for wettest conditions in each basin as a function of distance from a line connecting the Panamint and Bonneville basins**.** Line is shown in panel A. 95% confidence intervals are shown. Highstand ages are progressively younger with greater distance northwest from this line. See Supplementary Text for discussion of ages in the figure.

Data from other archives and for other Heinrich stadials are consistent with the patterns identified in HS1. Oxygen and uranium isotope data indicate increased precipitation in northern Utah's Bonneville Basin during HS2[29]. Speleothems in Arizona and New Mexico show decreases in $\delta^{18}O$ values during stadials throughout the last glacial cycle, consistent with an increase in winter precipitation and/or a decrease in summer precipitation during these events[18,19]. Tracers of local infiltration (growth rate, trace element concentrations, Sr isotopes, and/or $\delta^{13}C$ values) from stalagmites in eastern Nevada[30] and the central Sierra Nevada[31] indicate wetter conditions during HS11 and HS6, respectively, followed by rapid drying at the end of each stadial. In contrast, stadials appear to be marked by drier conditions in the Chewaucan basin of southeastern Oregon[32]. Together, these findings suggest that stadials prior to HS1 were also marked by greater winter precipitation in the southwest, central and northeast Great Basin, with drying in the northwest, consistent with a southwest-northeast orientation of anomalous moisture transport.

Relating western U.S. precipitation changes to atmospheric circulation during Heinrich stadials

We now investigate the relevant physical mechanisms using four freshwater hosing experiments performed with the fully coupled Earth system model CM2Mc, in which the atmospheric CO_2 concentration, ice sheets, and sea level provided for the LGM by the PMIP3 protocol are prescribed[33]. These experiments are run in four different orbital configurations, for opposite phases of obliquity ("Hi" and "Lo") and precession ("Boreal" and "Austral", for the hemisphere with greater summer insolation). Hereafter, we refer to each experiment by its combination of obliquity and precession, e.g. “Hi-Boreal”. These orbital parameters produce different pole-to-equator temperature gradients and seasonal ITCZ positions in the climate prior to hosing that shape the responses to hosing. The different atmospheric circulation and precipitation changes observed in the experiments then allow us to explore the drivers of these changes.

We focus on December to February (DJF), as winter precipitation is the dominant control on stream flow and lake level in the Great Basin[34,35] and because speleothem[18,19] and pollen[36,37] data are inconsistent with the suggestion that increased summer precipitation drove lake highstands[22]. All hosing experiments show DJF precipitation increases extending over the central North Pacific toward western North America, reaching maximum values at the coast (Figure 2). There, the precipitation increase is about twofold larger and extends farther inland in the two Boreal simulations than in the Australs. The precipitation increase is paralleled by near-surface (10 m) westerly and southwesterly wind anomalies in the eastern subtropical North Pacific that are stronger in the Boreals than in the Australs (Figure 2). These wind anomalies are accompanied by water vapor transport anomalies (not shown), suggesting that increased southwestern US precipitation in the Boreals is related to increased atmospheric river-like transport from subtropical latitudes to the mid-latitudes of western North America[27], similar to wind and vapor transport anomalies associated with high-precipitation winters today[38].

Importantly, the southwesterly orientation of wind and vapor transport anomalies in the northeastern Pacific matches the spatio-temporal pattern identified in the ages of deglacial lake highstands in Figure 1, suggesting that the hosing experiments broadly represent the dynamics of western U.S. precipitation changes during Heinrich stadials.

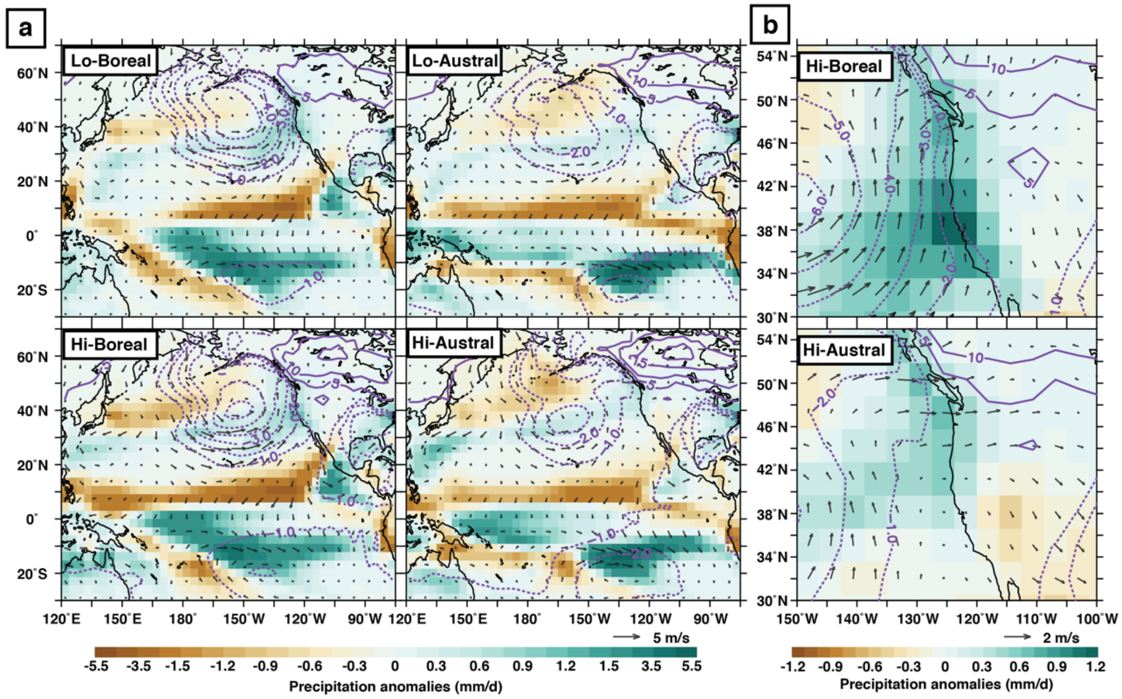

Figure 2. North Pacific precipitation and atmospheric circulation anomalies in hosing experiments. a) Anomalies in the DJF precipitation (mm/day; shading), near-surface (10 m) wind (m/s; arrows), and sea-level pressure (Pa; contours) between each hosing experiment and its corresponding control. **b)** As in **a**, but only for the simulations with the wettest (top) and driest (bottom) anomalies over the western US. Note that the shading color scale is adapted for a better view of the values over western North America. Contours are every 1 (5) Pa for negative (positive) pressure anomalies. Each experiment's name is given at the top left.

The southwesterly wind anomalies in the simulations are accompanied by SST and surface air temperature warming extending from the subtropics toward the southern Californian margin (Supplementary Figure 1), consistent with SST reconstructions indicating warming offshore southern California during Heinrich stadials[39].

The wind anomalies in the central and eastern North Pacific track along the southeastern margin of a large zone of negative sea-level pressure anomalies in the northeast Pacific, which represent the deepening and southeastward shift of the Aleutian Low in the hosings compared to the controls (Figure 2). Changes in the Aleutian Low are the largest in the Boreals, associated with the strongest wind anomalies in the northeast Pacific. These surface changes are accompanied by an intensification and slight southward shift of the jet stream over the North Pacific, as illustrated by the positive anomalies in the zonal wind at about 300 hPa (Figure 3 and Supplementary Figure 1, red contours); again, the changes are greater in the Boreals than in the Australs.

Two potential mechanisms can explain the jet stream intensification and Aleutian Low changes in the hosing experiments. On the one hand, anomalous cooling of the NH high latitudes due to AMOC shutdown and associated sea ice expansion increases the meridional temperature gradient between low- and high latitudes, which, in turn, enhances the upper-troposphere jet stream via thermal-wind adjustment. We find that this thermal-wind mechanism dominates in the North Atlantic basin, where colder temperature anomalies are accompanied by a stronger jet stream aloft (Supplementary Figures 1 and 2b). In the North Pacific, by contrast, the strongest jet anomalies are found in the two Boreals, even though high-latitude cooling and changes in the meridional temperature gradient are smaller in these simulations than in the Australs (Supplementary

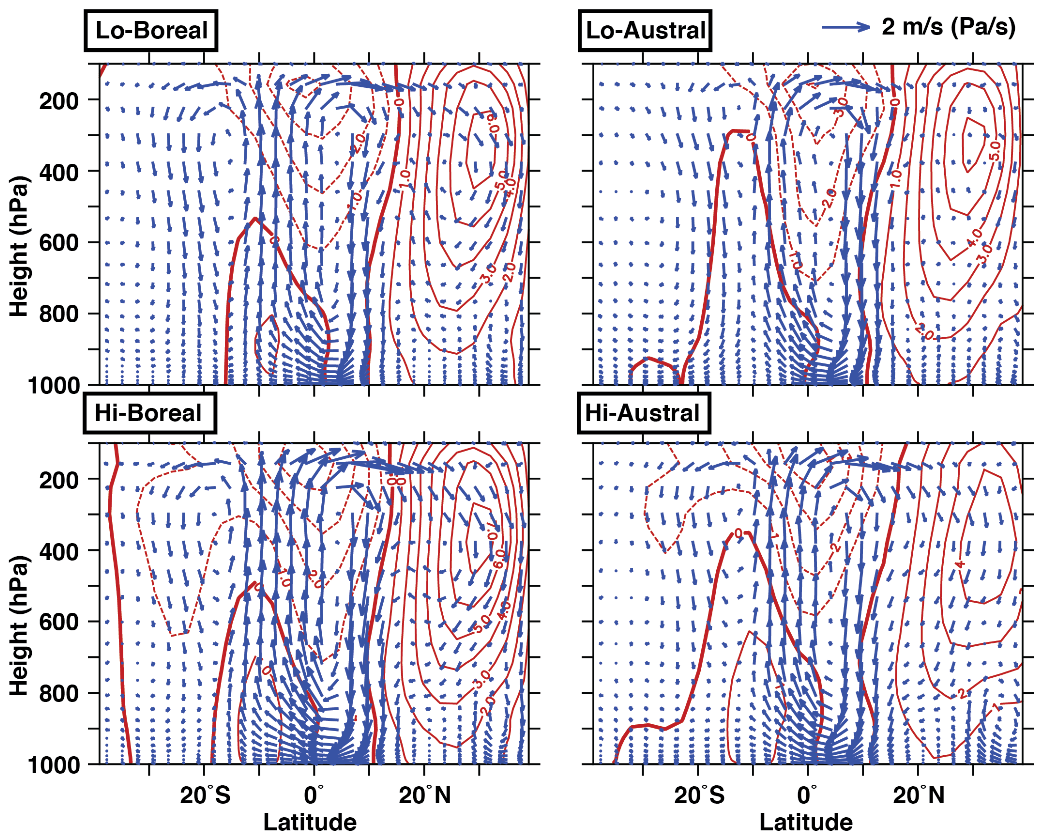

Figure 3. Central Pacific atmospheric circulation anomalies in the four hosing experiments. Anomalies in the DJF divergent wind and isobaric vertical velocity (blue vectors, in m/s and Pa/s respectively) and in DJF zonal winds (red contours, in m/s) between each hosing experiment and its corresponding control for the Pacific region between 120°E and 140°W. Isobaric vertical velocities are multiplied by 100 for a better view of the circulation cell vectors. Note the southward-shifted and larger Hadley cell anomalies and greater upper tropospheric jet anomalies in the Boreals (left panels).

Figures 1 and 2a). A previous modeling study also showed that the deepening of the Aleutian Low during Heinrich stadials is unlikely to be linked to high-latitude cooling, which in isolation would be expected to raise surface pressures throughout the mid- and high latitudes[23]. Another mechanism must therefore explain the jet and surface pressure anomalies in the North Pacific.

We propose that the mechanism instead involves the poleward transport of angular momentum by the Hadley circulation. In the hosing experiments, the AMOC shutdown leads to an inter-hemispheric heating contrast with anomalous cooling/warming in the NH/SH. To enhance the northward cross-equatorial atmospheric heat transport and thereby compensate the anomalous interhemispheric heating contrast, the ITCZ and the Hadley circulation shift southward[40]. The southward ITCZ shift intensifies the NH winter Hadley circulation, including in the North Pacific (Figure 3; blue arrows indicate changes in the wind field). This strengthening enhances the momentum convergence in the descending limb of the North Pacific Hadley circulation, thereby accelerating the jet stream.

In tandem with jet intensification, enhanced convergence in the subtropical central North Pacific acts as a wave source that alters stationary wave patterns to the north and east, leading to a deepening and southeastward shift of the Aleutian Low. This Aleutian Low response to anomalous convergence in the Pacific subtropics is well known from studies of Rossby wave propagation during El Niño events[41,42]; while Heinrich stadials differ from El Niño events in having opposite atmospheric responses in the NH and SH rather than hemispheric symmetry[43,44], both can intensify the North Pacific winter Hadley circulation[41,42], the central element in the mechanism described here.

As summarized schematically in Figure 4a, the jet and Aleutian Low responses to a stronger Hadley circulation increase southwesterly moisture transport into the western U.S.: increased westward momentum in the jet is ultimately transported downward to the surface by mid-latitude eddies, accelerating the low-level westerlies in the North Pacific (Figures 2 and 3), and the deepening and southeastward shift of the Aleutian Low drives southwesterly surface wind anomalies and increased water vapor transport into the southwestern U.S., as seen in modern interannual variability[38].

In contrast to the thermal-wind adjustment mechanism related to high latitude temperatures, the Hadley Cell momentum mechanism explains the differences in the anomalies in the North Pacific across the hosing experiments. In the simulations with larger precipitation increases in the southwestern U.S. (the Boreals), the central Pacific ITCZ shifts farther south and the Pacific winter Hadley circulation intensifies more (Figures 3, 4), converging more momentum into the subtropical central North Pacific (Supplementary Figure 3). This convergence transfers more momentum to the jet and elicits a stronger wave response in the northeastern Pacific, explaining why the larger ITCZ shifts in the Boreals are matched by greater jet and pressure anomalies (Figure 4b,c). The jet strengthening and the changes in the position and intensity of the Aleutian Low in turn lead to stronger near-surface westerly and southwesterly wind anomalies and, ultimately, to the largest precipitation anomalies over western North America (Figure 4d).

The hypothesized connection between the central Pacific and western U.S. lake levels is supported by recent reconstructions indicating large (~5˚) southward shifts of the central Pacific ITCZ during the major Heinrich stadials of the last two deglaciations

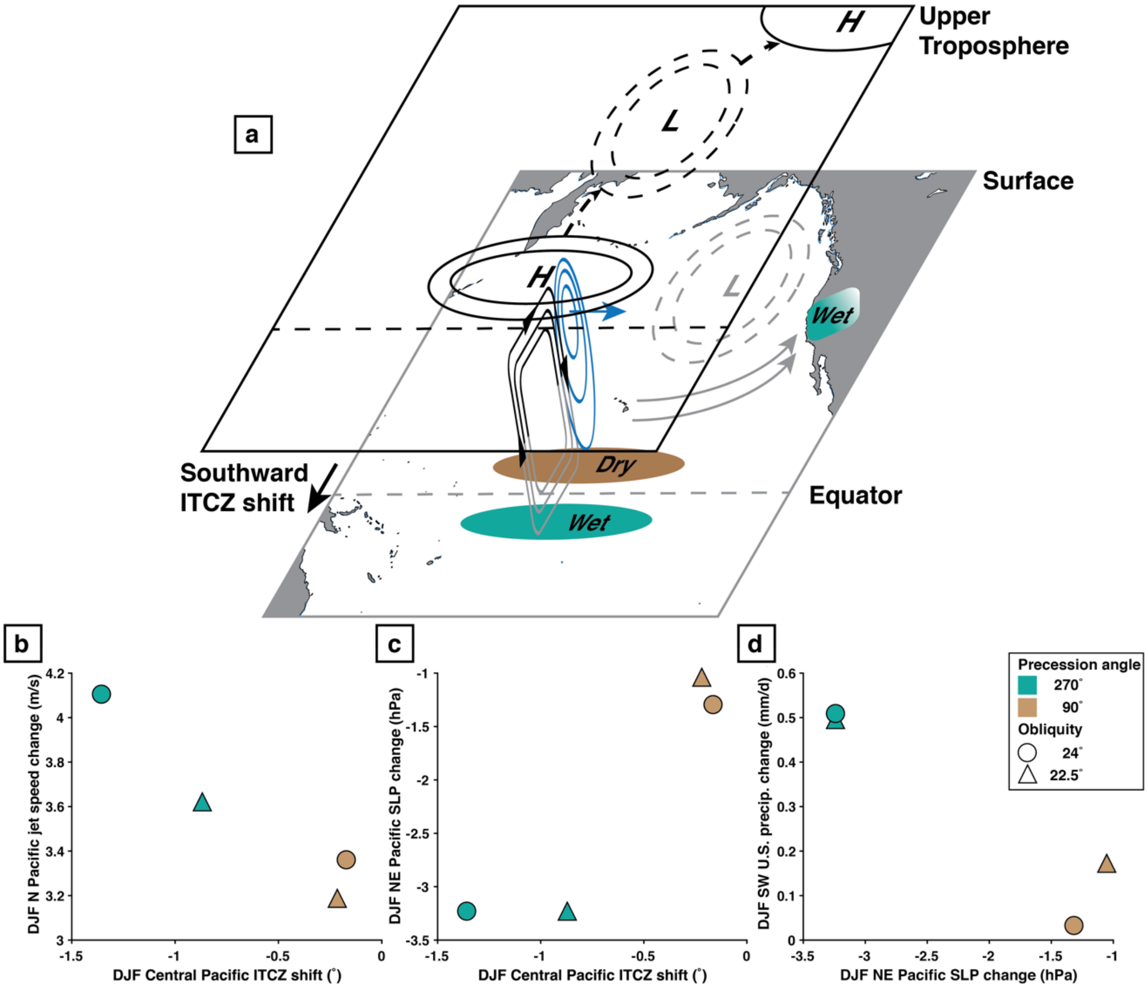

Figure 4. Dynamical links between central Pacific ITCZ shifts and increased southwestern U.S. precipitation during Heinrich stadials. a) Schematic diagram showing hypothesized surface (grey) and upper-level (black) Pacific atmospheric circulation changes during Heinrich stadials. The southward shift of the central Pacific ITCZ is accompanied by intensification of the NH winter Hadley circulation (streamlines), which intensifies the jet on its poleward edge (blue contours, blue arrow) and initiates a Rossby wave response extending through the NE Pacific (black contours showing pressure anomalies, dashed arrows) that causes the Aleutian Low to deepen and shift southeastward (grey dashed contours). Together these changes increase

southwesterly moisture transport into the southwestern U.S. and Great Basin (grey arrows). **b, c)** Scatter plots of **b)** DJF Pacific jet wind speed anomalies and **c)** DJF NE Pacific sea-level pressure (SLP) anomalies versus the shift in the DJF central Pacific ITCZ position in the hosing experiments relative to their respective controls, showing greater jet intensification and a deepening and eastward shift of the Aleutian Low in the experiments in which the ITCZ shifts farther south. **d)** Scatter plot of DJF southwestern U.S. precipitation anomalies versus DJF NE Pacific SLP anomalies in the hosing experiments, showing greater precipitation anomalies in the experiments with greater SLP responses, and thus in the experiments with greater ITCZ and jet changes. Green/brown symbols indicate precession angles of 270˚/90˚ (Boreal/Austral), and circles/triangles indicate obliquity angles of 24˚/22.5˚ (Hi/Lo).

(HS1, HS11)[45,46], substantially larger than estimates of global-mean ITCZ displacements[15]. Our analysis suggests that these southward shifts would have driven jet and Aleutian Low responses that, superimposed on the circulation effects of large remnant North American ice sheets, would have increased winter precipitation in the southwestern U.S. sufficiently to fill basins to their highstand levels. Our results offer strong support for the hypothesis that subtropical jet strengthening related to southward ITCZ shifts drove precipitation increases in the southwestern U.S. during Heinrich stadials[21], though our findings make clear that the Aleutian Low response is tightly linked and also plays a key role in the resulting precipitation changes. Our study agrees with the finding of consistent deepening of the Aleutian Low in response to hosing in a multi-model study[23], but we link Aleutian Low changes to convection anomalies in the tropical Pacific rather than in the western tropical Atlantic (Supplementary Text).

A remaining puzzle is why the central Pacific ITCZ shifts farther south in the Boreals than in the Australs. Most studies suggest that transport of anomalously cold, dry air by low-latitude winds is a central element both in communicating high-latitude cooling to the tropics and in driving zonal variability in ITCZ responses (e.g., ref. [47]), but connections of North Atlantic cooling to the central tropical Pacific have been relatively unexplored and remain an important target for investigation. One potential explanation of the larger shift in the Boreals is that the central Pacific winter ITCZ begins much farther south in the Austral control experiments than in the Boreals (Figure 4b), likely because of high DJF insolation in the Australs. Because northward heat transport associated with the Hadley circulation and the ocean's subtropical cells intensifies as the ITCZ shifts farther south[48,49], a southward-shifted ITCZ in the control simulation may migrate a shorter distance in response to perturbations such as hosing (Supplementary Figure 4).

An important implication of our results is that the central Pacific ITCZ position needs to be accurately simulated in order to capture the magnitude of western U.S. precipitation changes in response to climate perturbations. Climate models consistently show a southward bias in ITCZ position, particularly in the Pacific basin, under present-day conditions[50]. The mechanism identified here suggests that, in isolation, this bias should cause models to overestimate winter precipitation in the U.S. Great Basin and southwest prior to hosing, as observed in simulations of the modern climate[1]. Simulations of Northern Hemisphere cooling may underestimate the magnitudes of North Pacific atmospheric changes and western U.S. winter precipitation anomalies if the ITCZ and Hadley circulation begin with a southward bias. Future work should explore quantitative data-model agreement for precipitation anomalies during Heinrich Stadial 1 to understand whether models match the magnitude and not just the sign of precipitation anomalies estimated from lake level records.

The tropical-extratropical linkages documented here highlight the fact that changes local to the North Atlantic can have global effects that are driven through the tropical Pacific, and they offer a substantial contribution to efforts to build a global picture of atmospheric reorganizations during Heinrich stadials. We focus on the response in the North Pacific and western U.S., but the changes in the central Pacific ITCZ and Hadley circulation implicated here are likely to have had substantial impacts in the mid- and high latitudes of the Southern Hemisphere as well, through weakening of the SH Pacific subtropical jet and propagation of Rossby waves[21,51]. The mechanism also provides an important template for future data collection in the western U.S. and beyond, as the development of new well-dated hydroclimate records can offer additional tests of the spatial and temporal patterns we identify in presently available data.

Methods

Climate model experiments and data analysis

The four sets of simulations with the CM2Mc model use obliquities of 24˚ and 22.5˚ ("Hi" and "Lo") and precession angles of 270˚ and 90˚ between perihelion and autumnal equinox, with 270˚ corresponding to maximum NH seasonality/minimum SH seasonality and 90˚ to the opposite ("Boreal" and "Austral", respectively, for the hemisphere experiencing higher summer insolation). The eccentricity is held constant at 0.03. The hosing is applied as a uniform 0.2 Sv freshwater input in the North Atlantic for 1000 years, aiming to shut down the AMOC, as commonly done to simulate Heinrich stadials. For each experiment, we take the mean state of a 100-year-long period and compare it with a corresponding control simulation that is run under the same boundary conditions without hosing.

Variables in the scatter plots in Figure 4 are defined as follows: Pacific ITCZ position is the centroid of the precipitation rate between 20°S–20°N, zonally averaged between 120°E–140°W; the Pacific jet stream speed is the maximum of the zonal wind at 300 hPa averaged between 120°E–140°W; NE Pacific SLP is averaged over 30-60˚N, 120˚W-180˚; SW U.S. precipitation is averaged over 32-45˚N, 110-130˚W.

Acknowledgements

We thank Kenneth Adams for assistance in preparing Figure 1A. D.M. acknowledges support from NSF award EAR-1103379. JM and EMC acknowledge support from NOAA award NA16OAR4310177. EDG acknowledges support from Compute Canada award ayu-503 and Canadian Foundation for Innovation award 25402 and from the Spanish Ministry of Economy and Competitiveness, through the María de Maeztu Programme for Centres/Units of Excellence in R&D (MDM-2015-0552).

Author contributions

D.M. conceived the project and compiled paleo-data; E.M.C. analyzed the model output; E.G. conducted the model simulations; all authors contributed to interpreting the results; D.M. and E.M.C. wrote the manuscript with contributions from all authors.

Competing Interests statement

The authors declare no competing interests.

References cited

1. Seager, R. *et al.* Dynamical and thermodynamical causes of large-scale changes in the hydrological cycle over North America in response to global warming. *J. Clim.* **27,** 7921–7948 (2014).
2. Simpson, I. R., Seager, R., Ting, M. & Shaw, T. A. Causes of change in Northern Hemisphere winter meridional winds and regional hydroclimate. *Nat. Clim. Chang.* **6,** 65–70 (2016).
3. Russell, J. C. *Geological history of Lake Lahontan*. (U.S. Geological Survey Monograph 11, 1885).
4. Gilbert, G. K. *Lake Bonneville*. *U.S. Geological Survey Monograph 1* (U.S. Geological Survey Monograph 1, 1890).
5. Barth, C. *et al.* Late Pleistocene climate inferences from a water balance model of Jakes Valley, Nevada (USA). *J. Paleolimnol.* 1–14 (2016). doi:10.1007/s10933-016-9897-z
6. Ibarra, D. E., Egger, A. E., Weaver, K. L., Harris, C. R. & Maher, K. Rise and fall of late Pleistocene pluvial lakes in response to reduced evaporation and

precipitation: Evidence from Lake Surprise, California. *Geol. Soc. Am. Bull.* **126,** 1387–1415 (2014).
7. Hostetler, S. & Benson, L. V. Paleoclimatic implications of the high stand of Lake Lahontan derived from models of evaporation and lake level. *Clim. Dyn.* **4,** 207–217 (1990).
8. Harrison, S. P. *et al.* Evaluation of CMIP5 palaeo-simulations to improve climate projections. *Nat. Clim. Chang.* **5,** 735–743 (2015).
9. Antevs, E. The Great Basin, with emphasis on glacial and post-glacial times; climate changes and pre-white man. *Bull Univ Utah Biol. Ser* **19,** 168–191 (1948).
10. COHMAP. Climatic Changes of the last 18,000 Years: Observations and Model Simulations. *Science (80-.).* **241,** 1043–1052 (1988).
11. Bromwich, D. H. *et al.* Polar MM5 simulations of the winter climate of the Laurentide Ice Sheet at the LGM. *J. Clim.* **17,** 3415–3433 (2004).
12. Benson, L. V. *et al.* Chronology of expansion and contraction of four great Basin lake systems during the past 35,000 years. *Palaeogeogr. Palaeoclimatol. Palaeoecol.* **78,** 241–286 (1990).
13. Munroe, J. S. & Laabs, B. J. C. Temporal correspondence between pluvial lake highstands in the southwestern US and Heinrich Event 1. *J. Quat. Sci.* **28,** 49–58 (2013).
14. Putnam, A. E. A glacial zephyr. *Nat. Geosci.* **8,** 175–176 (2015).
15. McGee, D., Donohoe, A., Marshall, J. & Ferreira, D. Changes in ITCZ location and cross-equatorial heat transport at the Last Glacial Maximum, Heinrich Stadial 1, and the mid-Holocene. *Earth Planet. Sci. Lett.* **390,** 69–79 (2014).
16. Clark, P. U. *et al.* Global climate evolution during the last deglaciation. *Proc. Natl. Acad. Sci.* **109,** E1134–E1142 (2012).
17. Bard, E., Rostek, F., Turon, J.-L. & Gendreau, S. Hydrological Impact of Heinrich Events in the Subtropical Northeast Atlantic. *Science (80-.).* **289,** 1321–1324 (2000).
18. Asmerom, Y., Polyak, V. J. & Burns, S. J. Variable winter moisture in the southwestern United States linked to rapid glacial climate shifts. *Nat. Geosci.* **3,** 114–117 (2010).
19. Wagner, J. D. M. *et al.* Moisture variability in the southwestern United States linked to abrupt glacial climate change. *Nat. Geosci.* **3,** 110–113 (2010).
20. Lora, J. M., Mitchell, J. L. & Tripati, A. E. Abrupt reorganization of North Pacific and western North American climate during the last deglaciation. *Geophys. Res. Lett.* **43,** 11796–11804 (2016).
21. Chiang, J. C. H., Lee, S.-Y., Putnam, A. E. & Wang, X. South Pacific Split Jet, ITCZ shifts, and atmospheric North–South linkages during abrupt climate changes of the last glacial period. *Earth Planet. Sci. Lett.* **406,** 233–246 (2014).
22. Lyle, M. *et al.* Out of the Tropics: The Pacific, Great Basin Lakes, and Late Pleistocene Water Cycle in the Western United States. *Science (80-.).* **337,** 1629–1633 (2012).
23. Okumura, Y. M., Deser, C., Hu, A., Xie, S. P. & Timmermann, A. North Pacific climate response to freshwater forcing in the subarctic North Atlantic: Oceanic and atmospheric pathways. *J. Clim.* **22,** 1424–1445 (2009).
24. Adams, K. D. & Wesnousky, S. G. Shoreline processes and the age of the Lake

Lahontan highstand in the Jessup embayment, Nevada. *Geol. Soc. Am. Bull.* **110,** 1318–1332 (1998).

25. Benson, L. V *et al.* Correlation of late-Pleistocene lake-level oscillations in Mono Lake, California, with North Atlantic climate events. *Quat. Res.* **49,** 1–10 (1998).
26. Hudson, A. M. *et al.* Stable C, O and clumped isotope systematics and 14C geochronology of carbonates from the Quaternary Chewaucan closed-basin lake system, Great Basin, USA: implications for paleoenvironmental reconstructions using carbonates. *Geochim. Cosmochim. Acta* **212,** 274–302 (2017).
27. Lora, J. M., Mitchell, J. L., Risi, C. & Tripati, A. E. North Pacific atmospheric rivers and their influence on western North America at the Last Glacial Maximum. *Geophys. Res. Lett.* **44,** 1051–1059 (2017).
28. Oster, J. L., Ibarra, D. E., Winnick, M. J. & Maher, K. Steering of westerly storms over western North America at the Last Glacial Maximum. *Nat. Geosci.* **8,** 201–205 (2015).
29. McGee, D. *et al.* Lacustrine cave carbonates: Novel archives of paleohydrologic change in the Bonneville Basin (Utah, USA). *Earth Planet. Sci. Lett.* **351–352,** 182–194 (2012).
30. Cross, M. *et al.* Great Basin hydrology, paleoclimate, and connections with the North Atlantic: A speleothem stable isotope and trace element record from Lehman Caves, NV. *Quat. Sci. Rev.* **127,** 186–198 (2015).
31. Oster, J. L. *et al.* Millennial-scale variations in western Sierra Nevada precipitation during the last glacial cycle MIS 4/3 transition. *Quat. Res.* **82,** 236–248 (2014).
32. Zic, M., Negrini, R. M. & Wigand, P. E. Evidence of synchronous climate change across the Northern Hemisphere between the North Atlantic and the northwestern Great Basin, United States. *Geology* **30,** 635 (2002).
33. Brown, N. & Galbraith, E. D. Hosed vs. unhosed: Interruptions of the Atlantic Meridional Overturning Circulation in a global coupled model, with and without freshwater forcing. *Clim. Past* **12,** 1663–1679 (2016).
34. Cayan, D. & Peterson, D. H. The Influence of North Pacific Atmospheric Circulation on streamflow in the West. *Geophys. Monogr. 55, Am. Geophys. Union* 375–396 (1989). doi:10.1029/GM055p0375
35. Mann, M. E., Lall, U. & Saltzman, B. Decadal-to-centennial-scale climate variability: Insights into the rise and fall of the Great Salt Lake. *Geophys. Res. Let.* **22,** 937–940 (1995).
36. Heusser, L. E., Kirby, M. E. & Nichols, J. E. Pollen-based evidence of extreme drought during the last Glacial (32.6-9.0 ka) in coastal southern California. *Quat. Sci. Rev.* **126,** 242–253 (2015).
37. Holmgren, C. A., Norris, J. & Betancourt, J. L. Inferences about winter temperatures and summer rains from the late Quaternary record of C-4 perennial grasses and C-3 desert shrubs in the northern Chihuahuan Desert. *J. Quat. Sci.* **22,** 141–161 (2007).
38. Kim, H. M. & Alexander, M. A. ENSO's modulation of water vapor transport over the Pacific-North American Region. *J. Clim.* **28,** 3846–3856 (2015).
39. Pak, D. K., Lea, D. W. & Kennett, J. P. Millennial scale changes in sea surface temperature and ocean circulation in the northeast Pacific, 10-60 kyr BP. *Paleoceanography* **27,** 1–13 (2012).

40. Kang, S. M., Held, I. M., Frierson, D. M. W. & Zhao, M. The response of the ITCZ to extratropical thermal forcing: Idealized slab-ocean experiments with a GCM. *J. Clim.* **21,** 3521–3532 (2008).
41. Trenberth, K. E. *et al.* Progress during TOGA in understanding and modeling global teleconnections associated with tropical sea surface temperatures. *J. Geophys. Res.* **103,** 14291–14324 (1998).
42. Bjerknes, J. A possible response of the atmospheric Hadley circulation to equatorial anomalies of ocean temperature. *Tellus* **18,** 820–829 (1966).
43. Chiang, J. C. H. & Friedman, A. R. Extratropical Cooling, Interhemispheric Thermal Gradients, and Tropical Climate Change. *Annu. Rev. Earth Planet. Sci.* **40,** 383–412 (2012).
44. McGee, D. *et al.* Hemispherically asymmetric trade wind changes as signatures of past ITCZ shifts. *Quat. Sci. Rev.* **180,** 214–228 (2018).
45. Jacobel, A. W., McManus, J. F., Anderson, R. F. & Winckler, G. Large deglacial shifts of the Pacific Intertropical Convergence Zone. *Nat. Commun.* **7,** 10449 (2016).
46. Reimi, M. A. & Marcantonio, F. Constraints on the magnitude of the deglacial migration of the ITCZ in the Central Equatorial Pacific Ocean. *Earth Planet. Sci. Lett.* **453,** 1–8 (2016).
47. Liu, Y., Chiang, J. C. H., Chou, C. & Patricola, C. M. Atmospheric teleconnection mechanisms of extratropical North Atlantic SST influence on Sahel rainfall. *Clim. Dyn.* 1–15 (2014). doi:10.1007/s00382-014-2094-8
48. Donohoe, A., Marshall, J., Ferreira, D. & McGee, D. The Relationship between ITCZ Location and Cross-Equatorial Atmospheric Heat Transport: From the Seasonal Cycle to the Last Glacial Maximum. *J. Clim.* **26,** 3597–3618 (2013).
49. Green, B. & Marshall, J. Coupling of Trade Winds with Ocean Circulation Damps ITCZ Shifts. *J. Clim.* JCLI-D-16-0818.1 (2017). doi:10.1175/JCLI-D-16-0818.1
50. Oueslati, B. & Bellon, G. The double ITCZ bias in CMIP5 models: interaction between SST, large-scale circulation and precipitation. *Clim. Dyn.* **44,** 585–607 (2015).
51. Ding, Q., Steig, E. J., Battisti, D. S. & Küttel, M. Winter warming in West Antarctica caused by central tropical Pacific warming. *Nat. Geosci.* **4,** 398–403 (2011).
52. Reheis, M. C., Adams, K. D., Oviatt, C. G. & Bacon, S. N. Pluvial lakes in the Great Basin of the western United States—a view from the outcrop. *Quat. Sci. Rev.* **97,** 33–57 (2014).

Figure legends

Figure 1. Extents and ages of lake highstands in the U.S. Great Basin during the last deglaciation. a) Blue shading shows lakes at their greatest extents of the last glacial cycle. Colors denote timing of wettest conditions during the last deglaciation in each basin with sufficient dating confidence. Blue arrow shows direction of anomalous moisture transport during the first half of HS1 inferred from ages of lake highstands. Grey line is the outline of the Great Basin. Inset shows Great Basin outline with state boundaries. Paleolakes: B: Bonneville; Ch: Chewaucan; Cl: Clover; F: Franklin; J: Jakes; L: Lahontan; P: Panamint; R: Russell; S: Surprise; W: Waring. Lake highstand map adapted from [52]. **b)** Age estimates for wettest conditions in each basin as a function of distance from a line connecting the Panamint and Bonneville basins**.** Line is shown in panel A. 95% confidence intervals are shown. Highstand ages are progressively younger with greater distance northwest from this line. See Supplementary Text for discussion of ages in the figure.

Figure 2. North Pacific precipitation and atmospheric circulation anomalies in hosing experiments. a) Anomalies in the DJF precipitation (mm/day; shading), near-surface (10 m) wind (m/s; arrows), and sea-level pressure (Pa; contours) between each hosing experiment and its corresponding control. **b)** As in **a**, but only for the simulations with the wettest (top) and driest (bottom) anomalies over the western US. Note that the shading color scale is adapted for a better view of the values over western North America. Contours are every 1 (5) Pa for negative (positive) pressure anomalies. Each experiment's name is given at the top left.

Figure 3. Central Pacific atmospheric circulation anomalies in the four hosing experiments. Anomalies in the DJF divergent wind and isobaric vertical velocity (blue vectors, in m/s and Pa/s respectively) and in DJF zonal winds (red contours, in m/s) between each hosing experiment and its corresponding control for the Pacific region between 120°E and 140°W. Isobaric vertical velocities are multiplied by 100 for a better view of the circulation cell vectors. Note the southward-shifted and larger Hadley cell anomalies and greater upper tropospheric jet anomalies in the Boreals (left panels).

Figure 4. Dynamical links between central Pacific ITCZ shifts and increased southwestern U.S. precipitation during Heinrich stadials. a) Schematic diagram showing hypothesized surface (grey) and upper-level (black) Pacific atmospheric circulation changes during Heinrich stadials. The southward shift of the central Pacific ITCZ is accompanied by intensification of the NH winter Hadley circulation (streamlines), which intensifies the jet on its poleward edge (blue contours, blue arrow) and initiates a Rossby wave response extending through the NE Pacific (black contours showing pressure anomalies, dashed arrows) that causes the Aleutian Low to deepen and shift southeastward (grey dashed contours). Together these changes increase southwesterly moisture transport into the southwestern U.S. and Great Basin (grey arrows). **b, c)** Scatter plots of **b)** DJF Pacific jet wind speed anomalies and **c)** DJF NE Pacific sea-level pressure (SLP) anomalies versus the shift in the DJF central Pacific ITCZ position in the hosing experiments relative to their respective controls, showing greater jet intensification and a deepening and eastward shift of the Aleutian Low in the

experiments in which the ITCZ shifts farther south. **d)** Scatter plot of DJF southwestern U.S. precipitation anomalies versus DJF NE Pacific SLP anomalies in the hosing experiments, showing greater precipitation anomalies in the experiments with greater SLP responses, and thus in the experiments with greater ITCZ and jet changes. Green/brown symbols indicate precession angles of 270˚/90˚ (Boreal/Austral), and circles/triangles indicate obliquity angles of 24˚/22.5˚ (Hi/Lo).

Supplementary Text for "Tropical-extratropical linkages drove western United States lake expansions during Heinrich stadials" by D. McGee et al.

Estimates of highstand ages for lake basins

We combined recently published highstand age data with the data from a compilation of Great Basin highstand ages[1]. We include only ages that have been published in the peer-reviewed literature, and only include basins with more than one age on highstand samples or a well-developed lake level curve to test reproducibility. For basins that overflowed at their highstands and thus have extended periods at the highstand elevation, we have estimated the wettest period during the period of overflow (e.g., Bonneville) or left the overflowing basins out of the compilation and focused on data from downstream basins that received the overflow (e.g., Panamint). All radiocarbon ages are calibrated using INTCAL13, and uncertainties reflect the 95% confidence interval[2].

Bonneville Basin

Lake Bonneville overflowed from 18 ka to approximately 15 ka, first from the Bonneville shoreline level and then from the Provo shoreline level after the failure of the threshold lowered the spilling elevation by ~100 m (ref. [3]). $\delta^{18}O$ data from lake carbonates suggest that its wettest conditions were prior to 16 ka, as a rapid rise in $\delta^{18}O$ values beginning at 16 ka indicates an increase in water residence time in the basin[4,5]. The disappearance of dense deep-lake carbonate deposition from ~18-16.4 ka offers further support that the wettest (freshest) conditions occurred between 18-16 ka[5].

Chewaucan Basin

Three samples of shorezone tufa (lake carbonate) near the highstand shoreline were radiocarbon dated by Hudson et al.[6], producing ages ranging from 14.2±0.2 to 14.6±0.3 cal ka. These authors also present evidence that radiocarbon reservoir effects for the modern and past lake are likely to be negligible. Licciardi[7] radiocarbon dated four samples of aquatic gastropod shells associated with shorezone and near-shore deposits and found ages of 13-14 cal ka. These samples came from 30-35 m below the samples of Hudson et al., leading us to use the Hudson et al. results as the best estimate of the deglacial highstand age.

Clover Basin

Munroe and Laabs[1] collected five radiocarbon dates from aquatic gastropod shells from highstand beach ridges in the Clover Basin. The two samples from the ridge at the southern end of the basin produce ages of ~19.5 cal ka, suggesting a high lake in the basin at the LGM. The three samples from the northern end of the basin give a combined age of 17.3±0.2 cal ka, which we take as the best estimate of the age of the deglacial highstand.

Franklin Basin

Munroe and Laabs[8] presented five radiocarbon ages on aquatic gastropods from highstand shoreline deposits in the Franklin Basin and several ages on samples from lower shorelines. The highstand ages include one that is effectively infinite (>40 ^{14}C ka) and one that falls within the LGM; the authors indicate that both require replication before they can be further interpreted. The remaining three fall during a narrow window within Heinrich Stadial 1, ranging from 15.8±0.2 to 16.4±0.2 cal ka, with the possibility of a brief regression separating the older and younger dates.

Jakes Basin

García and Stokes[9] report a ^{14}C age of 16.8±0.2 cal ka for an aquatic gastropod sample from the highstand shoreline and a similar age for a result obtained through personal communication from K. Adams. Dating of gastropod samples from two recessional beach ridges just below the highstand shoreline produces ages in stratigraphic order that suggest abandonment of the highstand shoreline by 16.3±0.2 cal ka[9].

Lahontan Basin

A detailed lake level record for the Lahontan Basin has been developed by Benson et al.[10,11]. Radiocarbon dating of dense tufa coatings and lacustrine gastropods suggest that the lake highstand was attained for a brief period just after 16 cal ka[10,12]. A radiocarbon date on a camel bone within a highstand shoreline deposit provides the most precise date of the highstand, indicating that it occurred immediately prior to 15.7±0.2 cal ka[12].

Panamint Basin

The Panamint Basin was the terminal basin in the Owens River system during the pluvial maximum of the last deglaciation[13], so we focus on lake level changes in this basin rather than overflowing basins upstream (Owens, China, Searles). Jayko et al.[13] dated tufa and lacustrine shells from nearshore deposits in the Panamint Basin, finding that the highest lake levels during the deglaciation are recorded by samples dating to 17.0±0.3 cal ka and 17.2±0.3 ka. Slightly higher lake levels occurred during the last glacial maximum, which some authors attribute to the greater influence of evaporative demand at the southern end of the Great Basin[14].

Mono Basin (Lake Russell)

Radiocarbon dates from shoreline-associated tufas are presented by Benson et al.[15], and Benson et al.[16] integrate these results with data from sediment deposits in the basin. These results suggest that the highstand was short-lived. Munroe and Laabs[1] interpolate these results to suggest that the best estimate of the highstand age is 15.7±0.2 cal ka, though there remains some uncertainty about the radiocarbon reservoir age at the highstand elevation.

Surprise Basin

A detailed hydrograph for the LGM and deglacial history of Lake Surprise was developed by Ibarra et al.[17]. The authors determine that a tufa sample ^{14}C-dated to 15.2±0.2 cal ka provides the best estimate of the highstand age, and additional ^{14}C dates suggest sustained regression of the lake after this time. We use this estimate for the highstand age here, but we also note that U-Th and ^{14}C dates from the earlier portion of the deglaciation present an unclear picture of the lake history between ~18-15.2 ka, suggesting a need for further work to determine the duration of the highstand.

Goshute Valley (Lake Waring)

An aquatic gastropod sample from a highstand shoreline ridge from Pleistocene Lake Waring in the Goshute Valley was radiocarbon dated to 16.5±0.3 cal ka[1]. This age overlaps with the age of a highstand sample of 16.7±0.3 cal ka reported by García and Stokes[9]. We combine these two ages to produce a best estimate of 16.6±0.4 ka for the highstand.

Tropical Pacific vs. tropical Atlantic drivers of Aleutian Low response

Okumura et al.[18] found that the wintertime Aleutian Low consistently deepened in response to hosing in a comparison of simulations with four different fully coupled climate model simulations. Analyzing one model's response (CCSM2), they found that greater Aleutian Low deepening was associated with warmer before-hosing sea-surface temperatures in the tropical western North Atlantic; they thus suggested that the deepening of the Aleutian Low results primarily from anomalous propagation of Rossby waves from decreased atmospheric deep convection in the western tropical North Atlantic due to the hosing. Our results, however, do not fully support the proposed atmospheric bridge. The strongest deepening of the Aleutian Low occurs in the Boreals, which exhibit generally colder tropics than the Australs in both the control and hosed experiments and show smaller precipitation reductions in the Caribbean Sea in response to hosing. Further, our analysis emphasizes the importance of the southeastward shift of the Aleutian Low in addition to its overall deepening, as this shift draws southwesterly moisture transport into the southwestern U.S. rather than farther north. The Aleutian Low response in the CCSM2 results shown by Okumura et al. shows no evidence for a shift, as pressure anomalies are centered in the central North Pacific rather than the northeast Pacific[18]. It is unknown how the central Pacific Hadley circulation varied in the experiments in Okamura et al., and whether it agrees with our proposed mechanism; future work should investigate this response in hosing experiments conducted with different models.

References cited

1. Munroe, J. S. & Laabs, B. J. C. Temporal correspondence between pluvial lake highstands in the southwestern US and Heinrich Event 1. *J. Quat. Sci.* **28,** 49–58 (2013).
2. Reimer, P. *et al.* IntCal13 and Marine13 Radiocarbon Age Calibration Curves 0–50,000 Years cal BP. *Radiocarbon* **55,** (2013).
3. Oviatt, C. G. Chronology of Lake Bonneville, 30,000 to 10,000 yr B.P. *Quat. Sci. Rev.* **110,** 166–171 (2015).
4. Benson, L. V. *et al.* The rise and fall of Lake Bonneville between 45 and 10.5 ka. *Quat. Int.* **235,** 57–69 (2011).
5. McGee, D. *et al.* Lacustrine cave carbonates: Novel archives of paleohydrologic change in the Bonneville Basin (Utah, USA). *Earth Planet. Sci. Lett.* **351–352,** 182–194 (2012).
6. Hudson, A. M. *et al.* Stable C, O and clumped isotope systematics and14C geochronology of carbonates from the Quaternary Chewaucan closed-basin lake system, Great Basin, USA: Implications for paleoenvironmental reconstructions using carbonates. *Geochim. Cosmochim. Acta* **212,** 274–302 (2017).
7. Licciardi, J. M. Chronology of latest Pleistocene lake-level fluctuations in the pluvial Lake Chewaucan basin, Oregon, USA. *J. Quat. Sci.* **16,** 545–553 (2001).

8. Munroe, J. S. & Laabs, B. J. C. Latest Pleistocene history of pluvial Lake Franklin, northeastern Nevada, USA. *Bull. Geol. Soc. Am.* **125,** 322–342 (2013).
9. García, A. F. & Stokes, M. Late Pleistocene highstand and recession of a small, high-altitude pluvial lake, Jakes Valley, central Great Basin, USA. *Quat. Res.* **65,** 179–186 (2006).
10. Benson, L. *et al.* Insights from a synthesis of old and new climate- proxy data from the Pyramid and Winnemucca lake basins for the period 48 to 11 . 5 cal ka. *Quat. Int.* **310,** 62–82 (2013).
11. Benson, L., Kashgarian, M. & Rubin, M. Carbonate deposition, Pyramid Lake subbasin, Nevada: 2. Lake levels and polar jet stream positions reconstructed from radiocarbon ages and elevations of carbonates (tufas) deposited in the Lahontan basin. *Palaeogeogr. Palaeoclimatol. Palaeoecol.* **117,** 1–30 (1995).
12. Adams, K. D. & Wesnousky, S. G. Shoreline processes and the age of the Lake Lahontan highstand in the Jessup embayment, Nevada. *Geol. Soc. Am. Bull.* **110,** 1318–1332 (1998).
13. Jayko, A. S. *et al.* Late Pleistocene lakes and wetlands, Panamint Valley, Inyo County, California. *Geol. Soc. Am. Spec. Pap.* **439,** 151–184 (2008).
14. Reheis, M. C., Adams, K. D., Oviatt, C. G. & Bacon, S. N. Pluvial lakes in the Great Basin of the western United States—a view from the outcrop. *Quat. Sci. Rev.* **97,** 33–57 (2014).
15. Benson, L. V. *et al.* Chronology of expansion and contraction of four great Basin lake systems during the past 35,000 years. *Palaeogeogr. Palaeoclimatol. Palaeoecol.* **78,** 241–286 (1990).
16. Benson, L. V *et al.* Correlation of late-Pleistocene lake-level oscillations in Mono Lake, California, with North Atlantic climate events. *Quat. Res.* **49,** 1–10 (1998).
17. Ibarra, D. E., Egger, A. E., Weaver, K. L., Harris, C. R. & Maher, K. Rise and fall of late Pleistocene pluvial lakes in response to reduced evaporation and precipitation: Evidence from Lake Surprise, California. *Geol. Soc. Am. Bull.* **126,** 1387–1415 (2014).
18. Okumura, Y. M., Deser, C., Hu, A., Xie, S. P. & Timmermann, A. North Pacific climate response to freshwater forcing in the subarctic North Atlantic: Oceanic and atmospheric pathways. *J. Clim.* **22,** 1424–1445 (2009).

Supplementary Figures

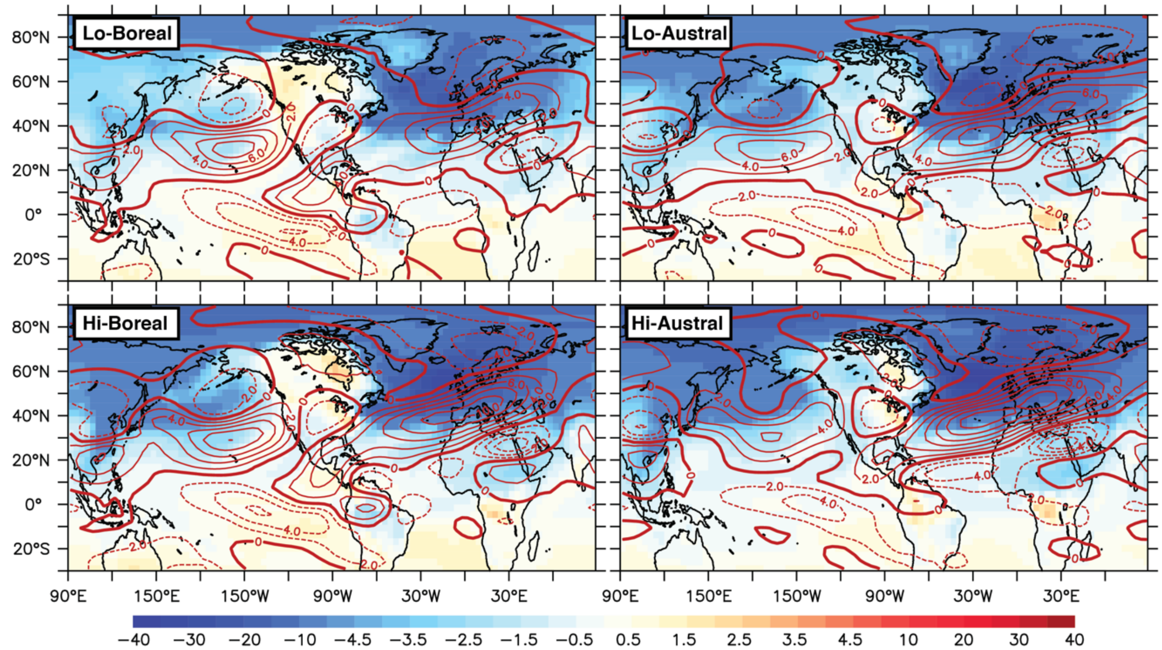

Supplementary Figure 1. Anomalies in the DJF near-surface (2 m) temperature (K; shading), and 300 hPa zonal wind (m/s; contours) between each hosing experiment and its corresponding control. Note that the color scale is nonlinear to allow a better view of the values over western North America.

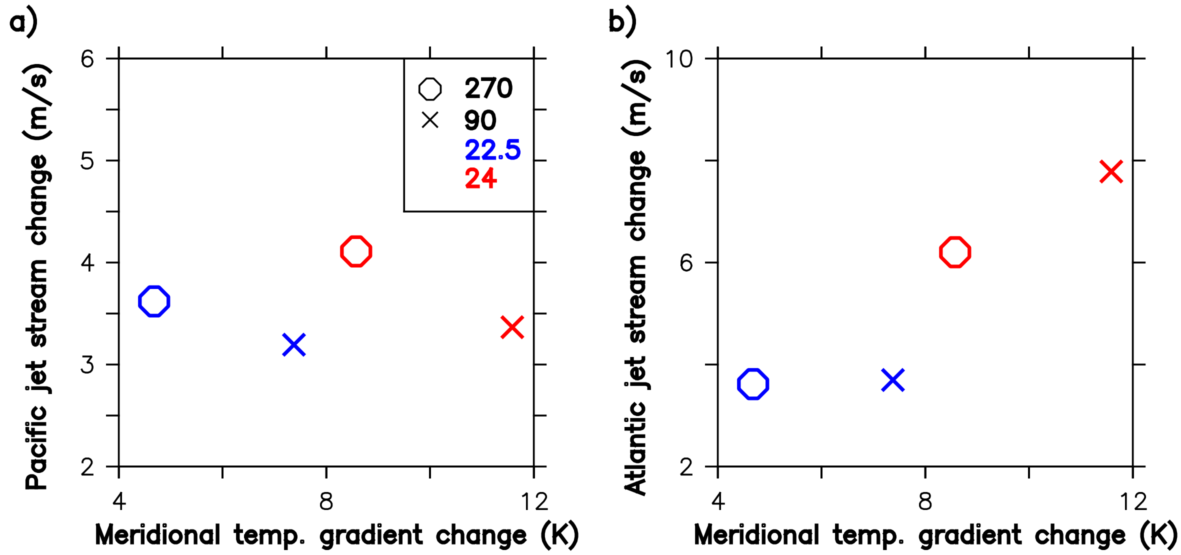

Supplementary Figure 2. Scatter plot of the change between the hosing and control experiments in the DJF **A)** Pacific and **B)** Atlantic jet stream versus the corresponding change in the DJF meridional temperature gradient. X's indicate simulations with 90˚ precession angle (Austral); circles indicate simulations with 270˚ precession angle (Boreal); and blue and red indicate 22.5˚ and 24˚ obliquity (Lo and Hi), respectively. The Pacific and Atlantic jets (in m/s) are defined as the maxima of the zonal wind at 300 hPa, averaged between 120°E and 140°W and between 80°W and 30°E respectively. The meridional temperature gradient is the difference in the zonally averaged global DJF surface air temperature between the Tropics (averaged between 30°S and 30°N) and NH high latitudes (between 60°N and 90°N). Note that the Atlantic jet becomes stronger as the meridional temperature gradient increases, but there is no clear relationship between the meridional temperature gradient and the Pacific jet.

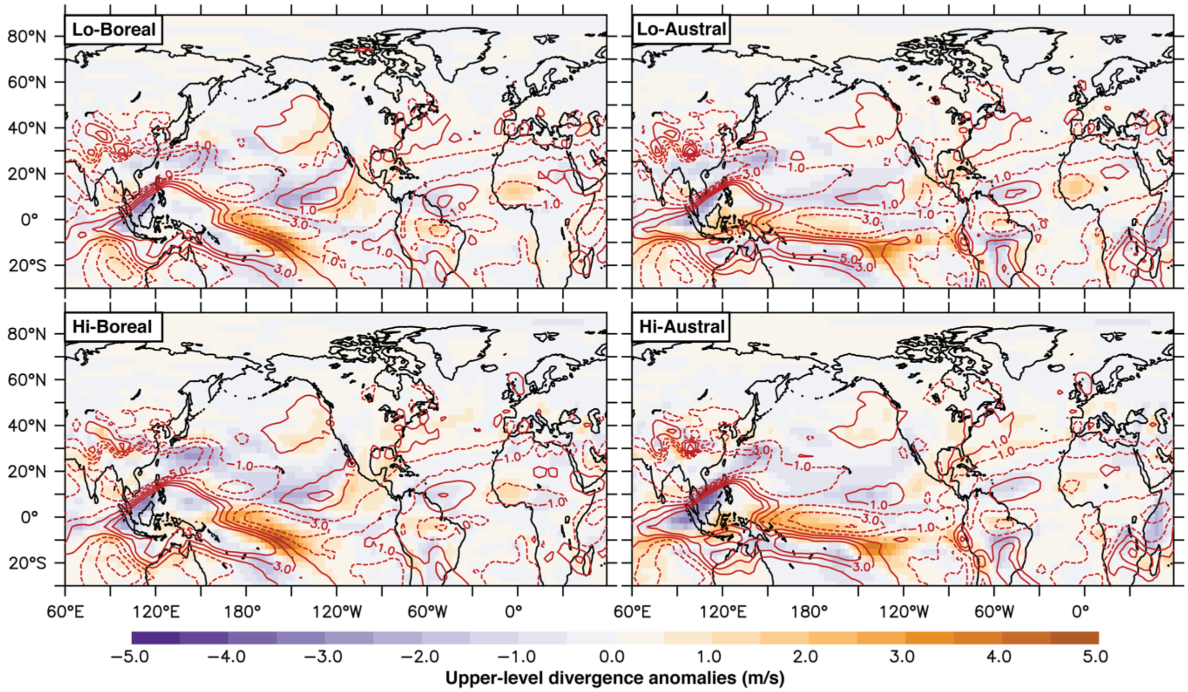

Supplementary Figure 3. Anomalies of upper-level (~150 hPa) DJF divergence (shading, with positive values indicating anomalous divergence and negative values indicating anomalous convergence; units are m/s) in response to hosing. Contours (m/s) show the mean DJF divergence in the respective glacial control simulations. All values are scaled by a factor of 10^6. Note the much stronger anomalous convergence in the subtropical central Pacific in the Boreals (left column) than in the Australs associated with the larger southward shift of the central Pacific ITCZ in the Boreals, driving the larger jet and Aleutian Low responses observed.

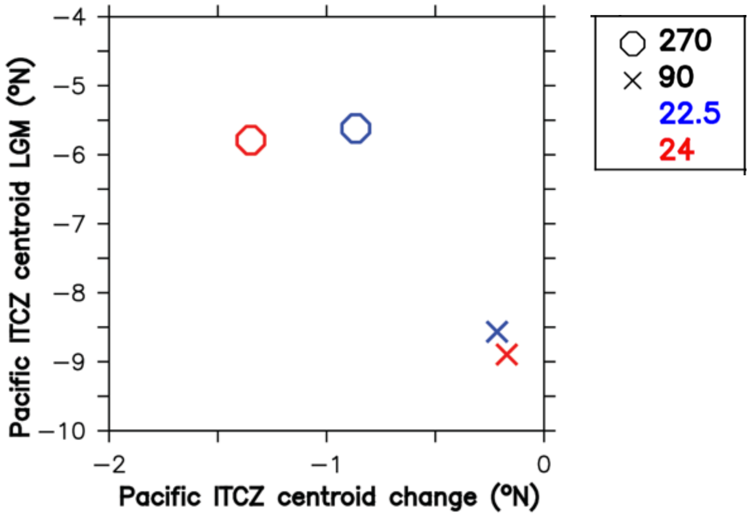

Supplementary Figure 4. Comparison of central Pacific DJF ITCZ shift in response to hosing (horizontal axis) to its position in the corresponding glacial control simulation. The ITCZ position is defined as in the caption to Figure 4. X's indicate simulations with 90˚ precession angle (Austral); circles indicate simulations with 270˚ precession angle (Boreal); and blue and red indicate 22.5˚ and 24˚ obliquity (Lo and Hi), respectively. Note that in the two Austral experiments experiments, the ITCZ starts farther south and shows smaller responses to hosing.